https://doi.org/10.18321/ectj959

Digital Modeling Accuracy of Direct Metal Laser Sintering Process

T. Dmitriyev[1,2]* and S. Manakov[2]

[1]Institute of Combustion Problems, 172 Bogenbai Batyr Str., Almaty, Kazakhstan
[2]al-Farabi Kazakh National University, 71 al-Farabi ave., Almaty, Kazakhstan

Article info

Received:
16 August 2019

Received in revised form:
4 November 2019

Accepted:
25 January 2020

Keywords:
Maraging steel
Metal additive manufacturing
Direct Metal Laser Sintering
Simulation
3D printing

Abstract

Products obtained by metal additive manufacturing have exceptional strength properties that can be compared with forged parts, and in some cases, even surpass them. Also, the cost and time of parts manufacture are reduced by two or even three times. Because of this, today's leading corporations in the field of aerospace industry introducing this technology to its production. To avoid loss of funds and time, the processes of additive manufacturing should be predictable. Simufact Additive is specialized software for additive manufacturing process simulation is dedicated to solving critical issues with metal 3D printing, including significantly reducing distortion; minimize residual stress to avoid failures; optimize the build-up orientation and the support structures. It also enables us to compare simulated parts with the printed sample or measure it as a reference. In other words, the simulated deformations can be estimated concerning the reference geometry. The current work aims to study the deformation of the sample during the Direct Metal Laser Sintering (DMLS) process made from Maraging Steel MS1. Simufact Additive software was used to simulate the printing process. The main idea is to compare the results of the simulation and the real model. EOS M290 metal 3D printer was used to make a test specimen.

1. Introduction

According to [1–4], the process of additive manufacturing (AM) is the method of material joining to produce a 3D object from digital data, generally layer upon layer. The most frequently used synonyms: additive layer manufacturing, additive processes, freeform fabrication [5]. This approach is the complete opposite of subtractive manufacturing, where for making parts, the material removes from the bulk substantial by grinding, milling, drilling, or carving. Due to the irreplaceable superiorities of AM in comparison to other manufacturing technologies, it has received considerable attention from both the commercial and academic sectors in the past few decades [6–8]. This technology allows printing various types of materials including metals [9–11], bioceramics [12–14], polymers [15], carbon based materials [16], and their composites.

*Corresponding author.
E-mail: timur_dmitriyev@yahoo.com

Today, there are several types of additive technologies, such as laser sintering, heterophase laser powder metallurgy, electron beam melting [13]. Laser technology for metal printing is by far the fastest-growing additive manufacturing method. As mentioned above, they can be divided into selective laser melting and direct laser growth. Selective laser melting (SLS) is a technology for manufacturing products of metal powders that are complex in shape and structure. First, a uniform layer of powder is formed on the substrate, and then the powder is melted using powerful laser radiation. The second type of additive manufacturing laser technology is so new that it does not yet have an established name: direct metal laser sintering (DMLS). Its principle lies in the fact that the metal powder is fed through a special nozzle directly into the same area where the laser beam is fed, forming a local bath of liquid melt [17]. Electron beam melting (EBM) is another additive manufacturing technology. This method is almost no different from metal SLS/DMLS printing.

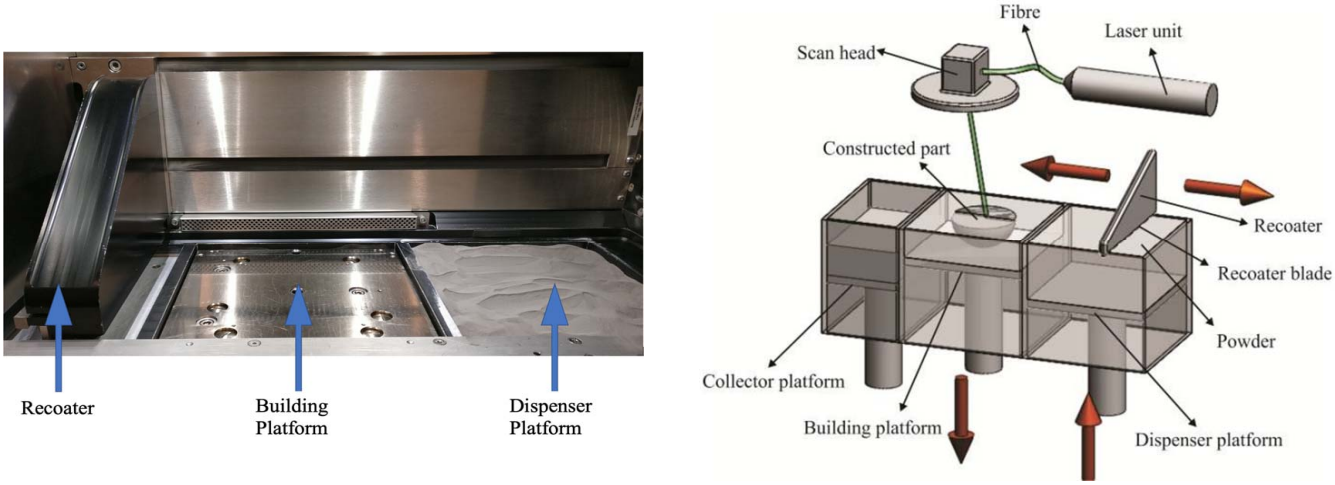

Fig. 1. Photograph of working chamber of DMLS machine and principal scheme of the process [21].

The only difference is that instead of a laser beam, melting is carried out using electric pulses. The technology of printing by electron beam melting of metal powders allowing to produce parts of almost any complexity, even tiny products with a size of 0.2–0.4 mm.

Nowadays, with the development of aerospace industry and parts manufacturing technologies, global science has focused on the development of additive manufacturing of metal products, the expansion of several metals and alloys, in particular nickel [16, 17] and titanium alloys [12, 18–20]. Also, it is worth noting that iron alloys take their place in metal additive manufacturing. For instance, works on sintering powders of maraging steel prove interested in this material.

Maraging steels are an ultra-high-strength iron alloy. The main alloying elements of such steels are nickel, cobalt, molybdenum, titanium, and aluminum. The high strength can be reached by precipitating intermetallic phases like Fe_2Mo, Ni_3 (Mo, Ti) while aging heat-treatment.

This paper is dedicated to the comparative analysis of the digital simulation of DMLS process with the physical process of obtaining metal 3D structures.

2. Materials and Methods

The experiment was performed on EOS M290 machine in a nitrogen atmosphere. The pre-heated up to 40 °C base plate is located inside the building chamber where the content of oxygen was below 1.3%. Default process parameters were used, where the scan speed and laser power were in the range of 400–2400 mm/s and 100–285 W, respectively. A zigzag pattern with 67° rotation between the adjoining layers was used for the laser scanning. The working principle is presented in Fig. 1.

According to [21] the specimen orientation should exclude a long line of parallel contact between recoating blade and printing part. Otherwise, it can lead to the damage of the specimen and/or recoating blade (driving motor). For the reduction of contact length, the part was rotated by an angle of 450. The overall time of the printing process was 1 h 18 min.

3. Results and Discussion

The physical characteristics were studied, including general dimensions of the object and surface roughness data of the UpSkin and DownSkin surfaces. The angled slope comparison analysis, as well as thickness analysis, showed pretty same results, so they were not included in this paper. For the investigation of material displacement eight angle slopes were made starting with 400, 450, 500, 550, 600, 700, 800 and 900.

In Fig. 2 there are pictures of part dimensions and support that were generated in Magics 20.04 software. The main objective of the work was the comparison and analysis of three types of samples: (a) – physical (printed); (b) – simulation of the as-built sample. The following are prescribed dimensions of the digital model: length – 80 mm, width – 10 mm, the thickness of the angled plate – 0.5 mm.

The printed specimen with support material is shown on Fig. 3. The picture shows the general view of the specimen with a support structure (brighter color under the object). The main function of the support material is the heat distribution during the object fabrication as well as providing comfortable detachment of the object from the base plate without destruction.

(a) 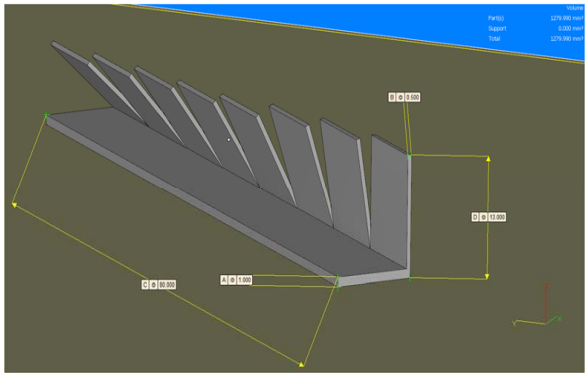 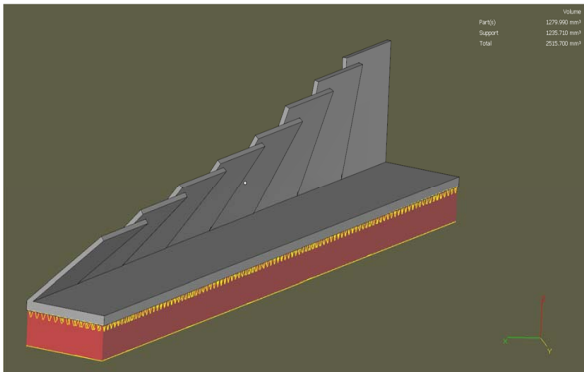 (b)

Fig. 2. Dimenstions of the specimen (a) with generated support (b)

 

Fig. 3. Photographs of printed specimen.

The dimensions of the printed sample are length – 79.93 mm, width – 9.93 mm, an average thickness of angled plate – 0.6 mm. As can be seen generally the dimensions are pretty similar. The slight differences appear due to internal stress during the process. This fact should be taken into account when fabricating high – precision objects by tolerance scope.

One of the main characteristics of materials fabricated by additive manufacturing is surface finishing also known as surface roughness. Surface roughness measurements of the specimen were carried out using Mitutoyo SJ-410 tester. The following parameters were evaluated: R_a – arithmetic average of the absolute values of profile deviations within the base length; R_z – sum of the average values of the absolute height profile of the five largest peaks and the depths of five largest cavities of profile within the base length.

$$R_a = \frac{1}{l} * \int_0^l |\, y(x) \,|\, dx \approx \frac{1}{n} * \sum_{i=1}^{n} |\, y_i \,| \qquad (1)$$

where l – the base length; n – the number of selected profile points on the base length; y – the deviation of the profile from the middle line.

$$R_Z = \frac{\sum_{i=1}^{5} |\, y_{pi} \,| + \sum_{i=1}^{5} |\, y_{vi} \,|}{5} \qquad (2)$$

where Y_{pi} – the height of the i-th largest protrusion of the profile; Y_{vi} – the depth of the i-th largest cavity of the profile.

Following is the Fig. (4a) that illustrates the example of the separate plot of microhardness calculation (Eqs. 1 and 2) and specimen photo (Fig. 4b) that indicates the Outer surface (UpSkin) and Inner surface (DownSkin).

(a) 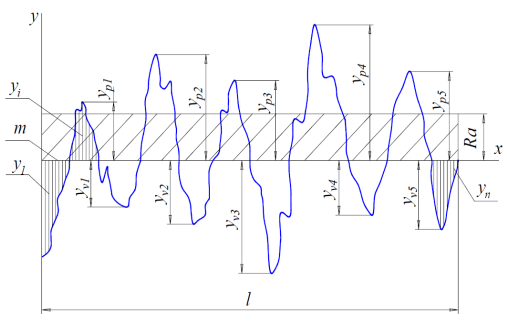 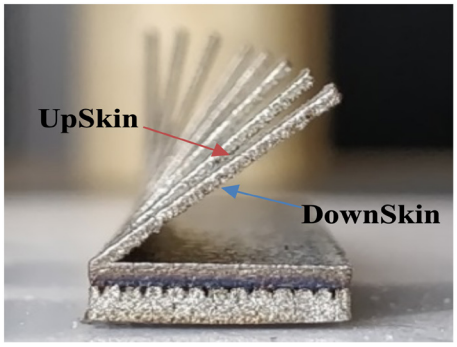 (b)

Fig. 4. Surface profile (a) and surface indication of the sample (b).

Since the surface roughness on the device had values in microinches, the following formula was used to convert the data into micrometers:

$$\mu m = \frac{\mu in}{39.37} \quad (3)$$

The results of surface roughness measurements are given in Table 1. Using Eq. 3 the obtained data was converted in micrometers.

Table 1
Sum of the average values (R_z) of the Inner Surface (Down Skin) roughness values and Outer surface (UpSkin) roughness

Angle, deg	UpSkin (µin)	DownSkin (µin)	UpSkin (µm)	DownSkin (µm)
40	1673.3	2128	46.4929	53.9572
	1927.92	2109.42		
	1890.06	2135.47		
45	2012.21	2272.52	54.7019	57.7369
	2202.63	2253.61		
	2246	2293.18		
50	1807.07	2543.59	45.2155	65.4718
	2066.73	2563.6		
	1466.6	2625.69		
55	1737.72	2424.57	45.6296	61.9644
	2238.38	2468.73		
	1413.21	2425.31		
60	2174.12	3063.21	54.0351	78.2722
	2004.56	3166.67		
	2203.41	3014.85		
70	1468.75	1508.67	37.5129	43.6548
	1357.32	1854.49		
	1604.58	1792.91		
80	1691.89	1592.3	46.8403	38.7101
	1757.56	1498.59		
	2082.86	1481.16		
90	1797	1358.71	42.3955	33.8843
	1680.32	1347.47		
	1530.01	1295.9		

To minimize the experimental errors, the measurements were carried out three times for each angle slope. Then the average value was taken.

As can be seen from Fig. 5 the surface roughness defers for UpSkin and DownSkin surfaces. The peak at 450 could be caused by measurement error that occur because measurements do not reflect the total roughness of the angled plate. Both peaks at 600 took place probably due to the uneven change in angle slope. The difference in surface roughness values of DownSkin and UpSkin could be explained by the differences in laser power and scanning speed parameters for both of them like. Moreover, during the printing process heat distributes through the part. With decreasing the slope angle of the printed part, the heat starts transferring through the nearby powder particles, which leads to powder adhesion onto the printing part. This fact determines the surface roughness of the specimen.

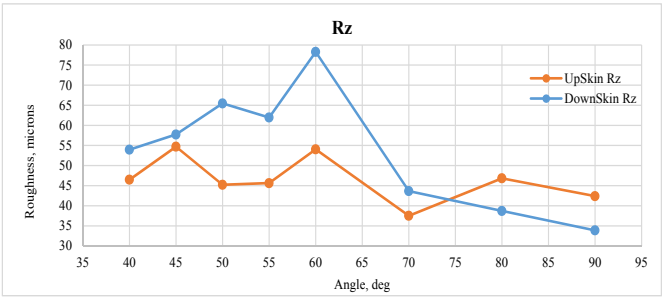

Fig. 5. Comparison between Inner and Outer surfaces roughness.

4. Conclusions

In this work, 18Ni-300 maraging steel MS1 test specimen was manufactured by DMLS process. The dimensions as well as the thickness of angled plates, and angle slopes were investigated by comparison between real printed sample and simulated model. Additionally, the surface roughness of the printed specimen was studied.

According to studies, the following conclusions can be drawn:

1. The values of sample dimensions and angle slopes measurements of the simulated model are pretty closely correlates with the printed specimen. It should be noted that the minimum feature size that can be reliably built with the given manufacturer machine settings is between 0.25 and 0.5 mm;

2. Surface roughness analysis showed inner and outer surface finishing is different because of deference in operating parameters of the printing process and heat distribution process. This fact could be described as with decreasing the slope angle of a printed specimen, the heat starts transferring through the nearby powder particles, which leads to powder adhesion onto the printing sample. This also leads to differences in the thickness of thin details of the manufactured sample.

Overall, simulated results have partially proved the prediction of the printing process, particularly dimensions and slope of angles. Although, the thickness values do not match the real specimen due to the complexity of the adhesion process of powder particles. The final goal of simulation of additive manufacturing is the creation of software that will make multiscale analysis on material structure, accuracy, part orientation changing and proper support structure generation. As result, such "ideal" model will be able to reduce to the minimum of raw material consumption and dramatically decrease the possibility of destruction of components during the printing process.

References

[1]. Y. Du, J. Chen, Q. Meng, Y. Dou, J. Xu, S.Z. Shen, *Vacuum* 178 (2020) 109384. DOI: 10.1016/j.vacuum.2020.109384

[2]. Z. Mansurov, *Eurasian Chem. Techn. J.* 18 (2016) 251–261. DOI: 10.18321/ectj482

[3]. C.A. Chatham, T.E. Long, C.B. Williams, *Prog. Polym. Sci.* 93 (2019) 68–95. DOI: 10.1016/j.progpolymsci.2019.03.003

[4]. Z. Mansurov, T. Dmitriyev, E. Aliyev, Ch. Daulbayev, Additive technologies (3D printing): monograph, Kazakh University, 2017, 192 p. ISBN: 978-601-04-3092-1 (in Russ.).

[5]. N. Horvath, A. Honeycutt, M.A. Davies, *CIRP Annals* 69 (2020) 509–512. DOI: 10.1016/j.cirp.2020.04.079

[6]. B. Alliot-Licht, A. Jean, M. Gregoire, *Arch. Oral Biol.* 39 (1994) 481–489. DOI: 10.1016/0003-9969(94)90144-9

[7]. V. Laghi, M. Palermo, G. Gasparini, V.A. Girelli, T. Trombetti, *J. Constr. Steel Res.* (2019) 105858 (in press). DOI: 10.1016/j.jcsr.2019.105858

[8]. M. Mazur, T. Bhatelia, B. Kuan, J. Patel, P.A. Webley, M. Brandt, V. Pareek, R. Utikar, *Chemical Engineering and Processing: Process Intensification* 143 (2019) 107595. DOI: 10.1016/j.cep.2019.107595

[9]. A. Li, X. Liu, X. Wan, Y. Yang, *Int. Commun. Heat Mass* 116 (2020) 104664. DOI: 10.1016/j.icheatmasstransfer.2020.104664

[10]. A. du Plessis, E. Macdonald, *Additive Manufacturing* 34 (2020) 101191. DOI: 10.1016/j.addma.2020.101191

[11]. E. Mirkoohi, D.E. Sievers, H. Garmestani, S.Y. Liang, *CIRP Journal of Manufacturing Science and Technology* 28 (2020) 52–67. DOI: 10.1016/j.cirpj.2020.01.002

[12]. D. Powell, A. Rennie, L. Geekie, N. Burns, *Journal of Cleaner Production* 268 (2020) 122077. DOI: 10.1016/j.jclepro.2020.122077

[13]. M. Kaminski, E. Loth, D.T. Griffith, C. (Chris) Qin, *Renew. Energ.* 148 (2020) 639–650. DOI: 10.1016/j.renene.2019.10.152

[14]. Z. Domagała, J. Domański, A. Zimmer, A. Tarczynska, J. Sliwa, B. Gworys, *Ann. Anat.* 228 (2020) 151436. DOI: 10.1016/j.aanat.2019.151436

[15]. H. Huang, W. Liu, Z. Liu, *CIRP Annals* 69 (2020) 33-36. DOI: 10.1016/j.cirp.2020.04.085

[16]. E. Cyr, A. Lloyd, M. Mohammadi, *J. Manuf. Process.* 35 (2018) 289–294. DOI: 10.1016/j.jmapro.2018.08.015

[17]. E.M. Sanfilippo, F. Belkadi, A. Bernard, *Computers Ind.* 109 (2019) 182–194. DOI: 10.1016/j.compind.2019.03.006

[18]. T. Grover, A. Pandey, S.T. Kumari, A. Awasthi, B. Singh, P. Dixit, P. Singhal, K.K. Saxena, *Materials Today: Proceedings* 26 (2020) 3071–3080. DOI: 10.1016/j.matpr.2020.02.636

[19]. D. Zindani, K. Kumar, *International Journal of Lightweight Materials and Manufacture* 2 (2019) 267–278. DOI: 10.1016/j.ijlmm.2019.08.004

[20]. L. Li, A. Haghighi, Y. Yang, *J. Manuf. Process.* 33 (2018) 150–160. DOI: 10.1016/j.jmapro.2018.05.008

[21]. National Institute of Standards and Technology Technical Note 1801, Lessons learned in establishing the NIST Metal Additive Manufacturing laboratory, (June 2013), 40 p. DOI: 10.6028/NIST.TN.1801